CrossMark

MRS Advances © 2017 Materials Research Society
DOI: 10.1557/adv.2017.433

Generic Graphene Based Components and Circuits for Millimeter Wave High Data-rate Communication Systems

Omid Habibpour[1], Wlodzimierz Strupinski[2], Niklas Rorsman[1], Pawel Ciepielewski[2] and Herbert Zirath[1]
[1]Microwave Electronics Laboratory, Department of Microtechnology and nanoscience, Chalmers University of Technology, 412 96 Göeborg, Sweden.
[2]Institute of Electronic Materials Technology, Wolczynska 133, 01-919 Warsaw, Poland.

ABSTRACT

We are developing millimeter wave (mm-wave) components and circuits based on hydrogen-intercalated graphene. The development covers epitaxial graphene growth, device fabrication, modelling, integrated circuit design and fabrication, and circuit characterizations. The focus of our work is to utilize the distinctive graphene properties and realize new components that can overcome some of the main challenges of existing mm-wave technologies in term of linearity.

INTRODUCTION

Graphene is a zero band-gap semiconductor with a linear band-structure. This unique band-structure gives rise to a very high carrier mobility and ambipolar behavior in graphene [1]. The lack of a bandgap limits maximum frequency of oscillation (f_{Max}) in Graphene field effect transistors (G-FETs). Therefore, the demonstrated G-FET based amplifiers have a low gain (< 10dB) and the operating frequencies are below 15 GHz [2-3]. However, the lack of a bandgap allows us to develop new G-FET based ultra-linear and wideband components capable of outperforming traditional technologies. G-FET based resistive mixers, modulators and demodulators operating at millimeter wave (mm-wave) are such promising components. In these components, G-FETs are biased in the linear region. The lack of a bandgap allows extending G-FET linear region to higher input power levels. In addition, it results in an odd symmetry in output characteristics of G-FETs, which enhances the linear behavior of G-FETs. Prior to our work, several G-FET based integrated circuit (IC) mixers have been demonstrated [4-5]. The operating frequency of these circuits are limited to a few GHz and they have a very narrow bandwidth. Our developed mixers operate at 80-100 GHz with a lowest reported conversion loss (17 dB).

In future mm-wave communication systems, the linearity of components will be the first priority. This is because, in a wideband system, the linearity can significantly affect major system level parameters such as receiver sensitivity and link budget. The linearity of current components such as mixers and power detectors based on existing technologies cannot satisfy future demands. Therefore, G-FET based components can play important roles in future wireless communication systems. In this paper, we present our work on developing generic G-FET components and circuits based on hydrogen-intercalated epitaxial graphene for high-data rate applications.

EXPERIMENTAL DETAILS

We are developing mm-wave components and circuits based on hydrogen-intercalated epitaxial graphene on silicon carbide substrate. Due to hydrogen intercalation, from the Hall data, graphene in this form exhibits a high carrier mobility (4000-8000 cm^2/Vs) at high carrier densities ($0.8\text{-}1.2\times10^{13}$ cm^2). This leads to low sheet resistance levels (200-250 Ω/ sqr) suitable for high frequency applications. We utilize bilayer graphene since a lower contact resistance (0.05 Ω·mm) is achievable. Figure 1a shows developed G-FETs with 250 nm gate-length. The fabricated G-FETs exhibit very high transconductances (1000-1200 mS/mm) and current density (2.5 A/mm). However, the cutoff frequency (f_T) is limited to 40 GHz due to high gate capacitance. Additionally, as can be seen in figure 1b, devices have a linear behavior because of lack of a bandgap. This limits maximum oscillation frequencies (f_{Max}). For 250 nm gate-length f_{max} of 30 GHz have been achieved which is far below the existing mature technologies. Therefore, we put our focus on applications where G-FETs operate in the linear region such as resistive mixers. For this application, using G-FETs is more beneficial than other FET technologies. This is because G-FET output characteristics is more linear and has an odd symmetry as opposed to conventional FETs. In addition, since FET resistive mixers are biased at zero voltage, 3-dB RF bandwidth is limited by switching time not f_T or f_{Max}. In our devices, it is about 250 GHz. To design our monolithic mm-wave integrated circuits (MMICs), an empirical G-FET model has been developed.

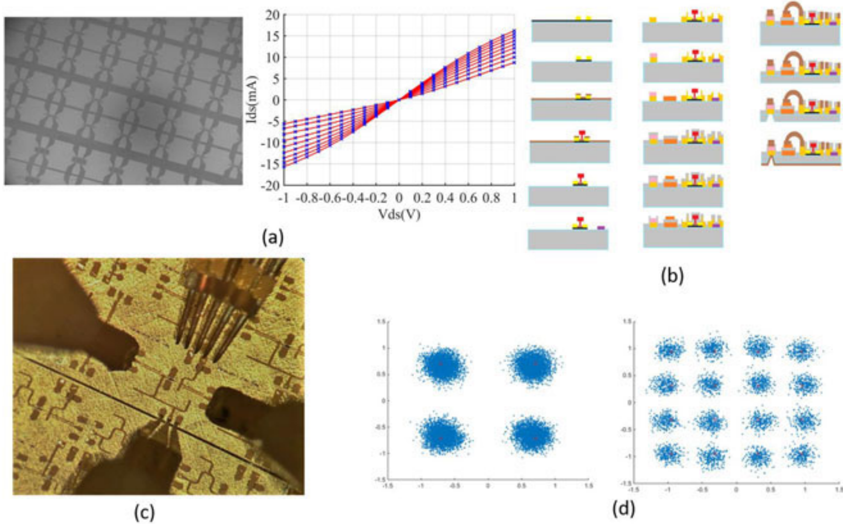

Figure 1. (a) Fabricated G-FET and its output characteristics with 250 nm gate-length (cross: measurement and solid line: model), (b) MMIC fabrication process steps (c) Fabricated MMIC mixers (d) I-Q constellation of up-converted 8 Gbps signal at 88 GHz (QPSK and 16 QAM)

The model can be implemented in standard circuit simulators such as Advanced Design System (ADS). Figure 1a shows the measurement and modeled data as well. It is seen that the model can predict the device behavior with good agreement. We have developed a complete MMIC fabrication process. Figure 1b shows the process chart including ebeam-lithography steps for G-FETs fabrication and photolithography steps for the fabrication of the passive elements and transmission lines. The chip is thinned down to 70 µm to suppress substrate modes and finally via holes are formed. The whole process can well preserve graphene transport properties [6]. Figure 1c illustrates the fabricated MMIC. The circuit is a single-ended resistive mixer operating at W-band (70-110 GHz) [7]. The mixer exhibits a flat conversion loss (CL) of 17-18 dB over measured frequencies of 80-100 GHz, which is among the lowest reported values for G-FET based mixers. However, the CL should be reduced by 6 dB for practical applications, which can be achieved by increasing the on-off ratio to 10-15. In addition, an input third-order intercept point (IIP3) of 20-25 dBm have been achieved which is a very promising result for a single-ended resistive mixer. Circuit simulation shows that by using a balanced mixer topology higher IIP3 (> 30 dBm) is achievable at W-band. This result appears to be state-of-the-art at mm-wave frequency. To further assess the linearity of the mixer, the circuit is used to up-convert high data-rate (8-16 Gbps) modulated signals. Figure 1d shows the constellation of the retrieved data. A bit error rate of 10^{-5} has been obtained. Additionally, it is seen than the constellation is not distorted suggesting that the mixer is highly linear [8].

DISCUSSION

Graphene has some unique properties as well as intrinsic drawbacks. Lack of a bandgap can limit utilizing graphene in many applications such as digital electronics and some RF applications like amplifiers. Effort in creating a bandgap (>0.2 eV) mainly results in damaging graphene mobility. Therefore, it is more beneficial to develop new high frequency technologies by exploiting the unique properties of *pristine* graphene. G-FET based linear and wideband mixers, modulator/demodulators and power detectors are such promising components for mm-wave applications. Ultra-linear and wideband components enable us to work over a wider frequency span. This eliminates the need for separate components for different frequency bands and consequently results in reducing cost and simplifying transmitter and receiver design. To use these graphene based components in practical applications there are some issues needed to be solved such as graphene uniformity for achieving a high yield fabrication as well as enhancing mixer CL.

Epitaxial Graphene Growth

In this study graphene is grown by traditional vapor phase epitaxy (VPE), widely applied in the electronic industry, using carbon precursor, i.e. methane [9]. This method enables the growth of carbon atomic layers directly on SiC surface with high the accuracy. Epitaxial graphene was grown at 1600 °C and 200 mbar pressure on 15x15 mm^2 nominally on-axis 6H-SiC (0001), Si-face semi-insulating chemo-mechanically polished substrates. Graphene layers are synthesized under an argon laminar flow at hot-wall Aixtron VP508 and Aixtron G5 WW reactors where graphene growth on 4″ SiC substrates was also developed. The process depends critically on the Reynolds number (Re) i.e. inertial and viscous force ratio, consequently

quantifying the relative importance of these two forces in a given gas flow. Tuning the value of the Re number allows to form a thick enough Ar boundary layer, which prevents Si sublimation. At the same time the diffusion of hydrocarbon to the SiC surface enables the growth of epitaxial mono- or bi-layer of graphene. To reduce the substrate effect on the synthesized graphene transport properties, hydrogen atoms are intercalated, which results in the formation of quasi-free-standing (QFS) graphene. It exhibits much higher and temperature independent carrier mobility, which is desirable for high-speed electronics. The carrier mobility and charge carrier concentration in our material are 6000-8500 cm^2/Vs and $8e12/cm^2$ [10, 11]. The intercalation of hydrogen is obtained in situ at the temperature of 1100 °C and 900 mbar pressure. The optimization of SiC surface high temperature (1600 °C) etching in hydrogen prior to the graphene growth due to controlling of the "step-bunching effect" enables to diminish the roughness down to 1nm, which means the eliminating of the atomic step edges and improving graphene uniformity within 4" wafer. This was confirmed by Raman measurements performed at room temperature in back scattering geometry with a Renishaw inVia Raman Microscope, using the 532 nm wavelength from Nd:YAG laser. The laser was focused on the sample using a x100 objective and a numerical aperture NA=0.9. Several spatial Raman maps were performed in the area of 20x20 microns with the distance of 0.7 microns between collected spectra.

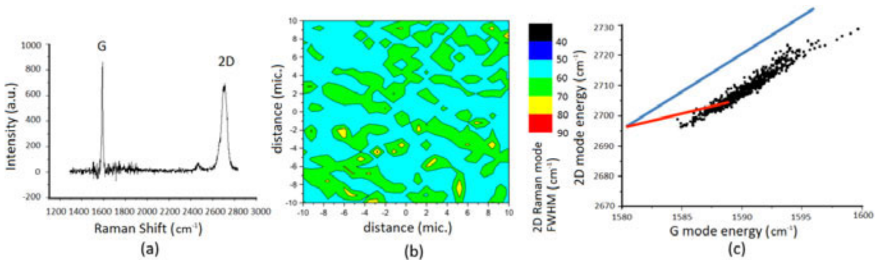

Figure 2. The Raman spectrum of graphene grown on 4" SiC wafer using Aixtron G5 WW system (courtesy of Nano Carbon) (a) typical Raman spectrum for graphene bilayer, (b) high uniformity confirmed by a spatial map of the FWHM of 2D Raman mode, (c) a correlation between 2D and G modes energies indicating a good agreement to Hall data. Blue line – a prediction of E (2D) vs. E(G) resulting from the uniaxial strain [9], red line - E(2D) vs. E(G) for strain-free graphene with varying density of holes [10].

The typical Raman spectrum observed in the experiment (after subtraction of the two-phonon Raman band from SiC substrate) is presented in Fig.2. Characteristic asymmetrical shape of the 2D mode , its FWHM (about 50 cm^{-1}) and the intensity ratio $I(2D)/I(G)<1$, indicate two-layers graphene structure with a Bernal stacking order [12]. The lack of the Raman defect mode, D peak around 1350 cm^{-1}, proves low defects concentration in graphene directly influencing transport properties. The spatial map of the FWHM of 2D Raman mode presented in Fig2.b confirms high homogeneity of the graphene structure. The correlation between the energies of 2D and G modes (Fig.2 c) reveals a small compressive strain in graphene [13] and the value of carrier concentration about 8E12 cm^{-2} which is in a good agreement with the Hall data [14].

CONCLUSIONS

This study presents one of the promising graphene applications that can outperform the traditional technologies. By combination of the unique properties of hydrogen-intercalated graphene and new device concepts, we have developed very linear and wideband components needed for future high data-rate communications.

ACKNOWLEDGMENTS

This work has been supported by the European Union's Horizon 2020 research and innovation program under grant agreement 696656. Graphene growth experiments have been performed using Aixtron G5 WW system owned by Nano Carbon, Poland.

REFERENCES

1. H. Castro Neto, F. Guinea, N. M. R. Peres, K. S. Novoselov, and A. K. Geim, Rev. Mod. Phys., 81, pp. 109–162, (2009).
2. C. Yu, Z. Z. He, Q. B. Liu, X. B. Song, P. Xu, T. T. Han, J. Li, Z. H. Feng, and S. J. Cai, IEEE Electron Device Letters, pp. 684-687, no. 5, (2016).
3. T. Hanna, N. Deltimple, M.S. Khenissa, E. Pallecchi, H. Happy and S. Frégonèse, Solid-State Electronics, 26-31, 127, (2017).
4. Yu-Ming Lin, Alberto Valdes-Garcia, Shu-Jen Han, Damon B. Farmer, Inanc Meric, Yanning Sun, Yanqing Wu, Christos Dimitrakopoulos, Alfred Grill, Phaedon Avouris,Keith and A. Jenkins, Science 332, 1294-1297 (2011).
5. S.J. Han, A. V. Garcia, S. Oida, K. A. Jenkins and W. Haensch, Nature Communications,
6. O. Habibpour, N. Rorsman and H. Zirath, Microwave Conference (APMC), (2015).
7. O. Habibpour, Z. S. He, W. Strupinski, N. Rorsman, T. Ciuk, P. Ciepielewski and H. Zirath, IEEE microwave and wireless components letter, pp. 168-170, no. 2, (2017).
8. O. Habibpour, Z. S. He, W. Strupinski, N. Rorsman, and H. Zirath, Scientific report, 7, 41828, (2017).
9. W. Strupinski, K. Grodecki, A. Wysmolek, R. Stepniewski, T. Szkopek, P. E. Gaskell, A. Grüneis, D. Haberer, R. Bozek, J. Krupka and J. M. Baranowski, Nano Lett., 11, 1786–91 (2011).
10. T. Ciuk, S. Cakmakyapan, E. Ozbay, P. Caban, K. Grodecki, A. Krajewska, I. Pasternak, J. Szmidt, and W. Strupinski, J. App. Phys. 116, 123708 (2014)
11. C. Riedl, U. Starke, J. Bernhardt, M. Franke and K. Heinz, Phys. Rev. B, 76, 245406 (2007).
12. A. C. Ferrari, J. C. Meyer, V.Scardaci, C. Casiraghi, M. Lazzeri, F. Mauri, S. Piscanec, D. Jiang, K. S. Novoselov, S. Roth, and A. K. Geim, PRL 97, 187401 (2006).
13. T. M. G. Mohiuddin, A. Lombardo, R. R. Nair, A. Bonetti, G. Savini, R. Jalil, N. Bonini, D. M. Basko, C. Galiotis, N. Marzari, K. S. Novoselov, A. K. Geim, A. C. Ferrari, Phys. Rev. B, 70 (20) 205433 (2009).

14. A. Das, S. Pisana, B. Chakraborty, S. Piscanec, S. K .Saha, U. V. Waghmare, K. S. Novoselov, H. R. Krishnamurthy, A. K. Geim, A. C. Ferrari, A. K. Sood, Nature Nanotech. 3, 210 (2008).